PREDICTING THE BEHAVIOR OF AI AGENTS USING TRANSFER OPERATORS

Anonymous authors
Paper under double-blind review

ABSTRACT

Predicting the behavior of AI-driven agents is particularly challenging without a preexisting model. In our paper, we address this by treating AI agents as stochastic nonlinear dynamical systems and adopting a probabilistic perspective to predict their statistical behavior using the Fokker-Planck equation. We formulate the approximation of the density transfer operator as an entropy minimization problem, which can be solved by leveraging the Markovian property and decomposing its spectrum. Our data-driven methodology simultaneously approximates the Markov operator to perform prediction of the evolution of the agents and also predicts the terminal probability density of AI agents, such as robotic systems and generative models. We demonstrate the effectiveness of our prediction model through extensive experiments on practical systems driven by AI algorithms.

1 INTRODUCTION

Autonomous agents operate in dynamic environments, making decisions based on continuous feedback that enables them to learn and adapt over time. Therefore, studying the behavior and alignment of these AI-driven agents is critical for several reasons. Analyzing their actions can help prevent behaviors that conflict with human values and ethical standards [Rossi & Mattei (2019), Doshi & Gmytrasiewicz (2005)]. Furthermore, understanding their behavior is essential for enhancing their efficiency and reliability, particularly in safety-critical applications such as autonomous robots [Pourmehr & Dadkhah (2012)]. These intelligent models are typically complex, high-dimensional, and only partially observable over short time intervals. This complexity raises the question of which properties can be efficiently quantified to truly understand their capabilities. The design and understanding of AI components embedded within these agents depend crucially on analyzing the interplay between AI-driven decision-making and the physical behavior of the closed-loop system. This capability is foundational for users to perceive, predict, and interact effectively with intelligent systems. It also provides the theoretical and technical basis for practical tasks such as decision-making and reinforcement learning [Levine et al. (2016), Ganzfried & Sandholm (2011)].

Given these challenges, it is important to develop methods capable of harnessing critical information to identify the behavior of AI components in closed-loop systems. In Déletang et al. (2021) and Roy et al. (2022), the authors try to model the AI agent as a system that was pre-trained using reinforcement learning and the environment is a partially-observable Markov decision process. The authors in Dipta et al. (2022) present a card game and leverage the game theory framework to analyze learning agents' characteristics with environmental changes. Moreover, Lee & Popović (2010) try capture a rich set of behavior variations by determining the appropriate reward function in the reinforcement learning framework. For a comprehensive review of literature on modeling and predicting AI agents behavior, we refer readers to Albrecht & Stone (2018). Among these emerging methodologies, there has been a notable increase in modeling these behaviors as nonlinear dynamical systems [Narendra & Parthasarathy (1992); Beer (1995); Suttle et al. (2024); Ijspeert et al. (2002)]. Originating from studies in partial differential equations (PDEs) and fluid mechanics, techniques such as Dynamic Mode Decomposition (DMD) and its generalizations have also demonstrated significant capability in revealing the underlying evolutionary laws of AI agents [Schmid (2022), Brunton et al. (2021)].

Despite these advances made in the above mentioned works chaotic behavior resulting from nonlinearity and stochasticity encountered in practical problems pose significant challenges to deterministic

modeling and identification. However, despite the substantial uncertainties, and sensitivities to initial conditions affecting AI agents, their statistical behavior and properties can be surprisingly regular. Specifically, when the closed-loop dynamics of AI agents are time-invariant, the density evolution of the agents' states follows a Markovian property [Risken (1996), Gardiner (2009), Hoehn et al. (2005)].

These observations motivate analyzing this problem from a statistical perspective. In particular, modeling the evolution trajectories of the state via a stochastic process and then studying the transfer and propagation of the probability density functions, has gathered a lot of attention. This approach, drawing from statistical mechanics, assumes that the agents trajectories are independent and governed by the same Fokker-Planck equation, which characterizes the statistical behavior of agents based on their underlying dynamics, showing significant advantages in handling systems with complex, high-dimensional nonlinear chaotic dynamics and noise perturbations [Risken (1996); Lasota & Mackey (2013)]. Another motivation for analyzing the evolution of densities arises from generative AI. The characteristics of the sampling probability density are often intricate. Traditional statistical models frequently fall short due to the high dimensionality of the data and the inherent complexities of the sampling process. Generative models, such as those based on denoising diffusion processes [Ho et al. (2020)] or iterative reward-based sampling methods using transformers [Kingma (2013)], introduce complex stochastic dynamics. These dynamics are challenging to analyze at the level of individual samples. Instead, adopting a macroscopic perspective and focusing on the evolution of probability densities induced by these models enables the study of the aggregate behavior of complex models and a better understanding of their underlying mechanisms.

The application of probabilistic models to learn and predict the statistical behavior of complex AI agents has gained increasing attention in areas such as autonomous driving, motion planning, and human-robot interaction [Lefèvre et al. (2014); Trautman et al. (2015); Bai et al. (2015); Rasouli et al. (2017)]. However, algorithms based on this probabilistic perspective, particularly those studying the propagation of density processes, remain underexplored. Several open challenges persist in advancing this field, especially in developing unified frameworks that bridge the gap between domain-specific methodologies and general modeling approaches [Baarslag et al. (2016)].

In this work, we focus on virtual or physical agents with stochastic dynamics, which are controlled or operated by AI algorithms. We model the evolution of their state distributions as a Markov chain (or process). Unlike existing approaches that primarily predict agent evolution, our work adopts a macroscopic/statistical mechanics perspective. Our aim is to develop algorithms capable of predicting not only the propagation of future densities but also the stationary distribution of the Markov process, which corresponds to the controlled objective applied to the AI agents.

Specifically, we utilize the spectral decomposition theorem [Lasota & Mackey (2013)] for Markov operators to decompose the propagation of the Markov transfer operator into a transient decaying term and projections onto a set of cyclical bases representing the asymptotic behavior. As demonstrated in our analysis, this approach significantly simplifies the learning and representation of Markov processes, while also facilitating the prediction of the agents' future behavior from a macroscopic perspective.

1.1 Related Works

Here we review some empirical and theoretical models from a statistical modeling perspective that have been developed with the aim of improving the prediction of the behavior of agents with AI models in the loop. In Goswami et al. (2018), the constrained Ulam Dynamic Mode Decomposition method is presented to approximate the Perron-Frobenius operators for both the deterministic and the stochastic systems. Norton et al. (2018) provides a numerical approximation of the PF operators using the finite volume method. These early numerical methods lay very important foundations for the subsequent development of deep-learning-based methods, which turn out to be more scalable approaches. For example, Meng et al. (2022) provides a direct learning method by training a neural network-based state transfer function (operator). The works Huang et al. (2019); Everett et al. (2021); Zhang et al. (2023) estimate the reachability sets of neural network-controlled systems. The works Li et al. (2021) and De Ryck & Mishra (2022) use deep operator networks (DeepONets) and Fourier neural operators (FNOs) to approximate the solution trajectories of PDEs. More recently, Surasinghe et al. (2024) proposes an approximation method based on kernel density estimation (KDE) and

Hashimoto et al. (2024) present a deep reproducing kernel Hilbert module (deep-RKHM), serving as a deep learning framework for kernel methods. Beside the above-mentioned empirical methods, there are also some works that try to learn to statistical behavior from an optimal-transport-theory perspective. For example, in Yang et al. (2022), the authors seek to recover the parameters in dynamical systems with a single smoothly varying attractor by approximating the physical invariant measure. In Karimi & Georgiou (2022), the authors provided a data-driven approximation approach to the Perron-Frobenius operator using the Wasserstein Metric.

A formal analysis of agents with AI models in feedback from the perspective of the evolution of the density is currently lacking in the literature. Reachability analysis needs tracking of every possible trajectory which can be computationally expensive. The density evolution approach uses a single quantity that measures the probability of evolution of trajectories and offers a significant computational advantage. Further, the density perspective allows a convenient method to verify the alignment of machine learning models. We seek to address these challenges in this work.

1.2 Our Contributions

Our main contributions are as follows:

- AI-driven agents behave in unpredictable ways due to machine learning black boxes. We look at this through the lens of propagation of probability densities and the stochastic transfer operator. AI agents are trained with data that has inherent biases. This, coupled with the structure of machine learning models, can potentially alter the alignment of the model. To verify the alignment of the model, we predict the asymptotic behavior of the model by analyzing the terminal stationary density of the AI agents.
- We propose PISA, a novel and scalable algorithm that can simultaneously predict the evolution of the densities of AI agents and estimate their terminal density. Our algorithm is motivated by the spectral decomposition theorem [Lasota & Mackey (2013)] and provides a theoretical backing for its performance. PISA simultaneously approximates the action of the Markov transfer operator from the trajectory data of agents and predicts their asymptotic behavior.
- In our proposed algorithm PISA, the model complexity is indexed by the number of basis functions. The number of basis functions is a tunable parameter that can be altered according to the user's needs. We provide a theoretical guarantee of the existence of the optimal solution to our operator estimation problem.
- We numerically verify the effectiveness of PISA in a variety of practical cases and compare it with existing literature. We first predict the behavior of unicycle robots driven by a controller based on diffusion models. Then we analyze the behavior of generative models from the lens of density evolution. Lastly, we apply PISA in the case of predicting the movement of pedestrians. We observe that PISA performs significantly better than the existing literature.

1.3 Statistical Behavior Perspective and the Fokker-Planck Equation

Consider a practical AI agent with physical dynamics defined by

$$\dot{x} = h(x, u) + g(x)\xi, \tag{1}$$

where u is an external input to the system and ξ represents the white noise signal. With a parameterized machine learning model as feedback $u = \texttt{ML}_\theta(x)$, the system's dynamics including the feedback input is given by

$$\dot{x} = h(x, \texttt{ML}_\theta(x)) + g(x)\xi = f(x) + g(x)\xi, \tag{2}$$

where $x(t) \in X \subseteq \mathbb{R}^M$ and $f(\cdot) : \mathbb{R}^M \mapsto \mathbb{R}^M$ and $g(\cdot) : \mathbb{R}^M \mapsto \mathbb{R}^p$ are nonlinear continuous functions.

The nonlinear system (2) is highly dependent on initial conditions and the noise ξ. Instead of analyzing individual trajectories of (2), we take the perspective of analyzing several independent trajectories simultaneously. Despite the challenges posed by stochasticity, and complexity in the system dynamics, the evolution of the statistical distribution over the states of all agents remains

well-structured [Lasota & Mackey (2013)]. Particularly, at each time instance, samples from all the independent trajectories can be viewed as a probability density of the states. Therefore, the evolution of states from various initial conditions can be viewed as the evolution of a probability density. The evolution of the probability density function of states at time t, denoted by $\rho(x,t)$, forms a Markov process that obeys the Fokker-Planck equation, as described below:

Lemma 1 (Risken (1996)) *For agents governed by* (2)*, we have that the evolution of the density of states $\rho(x,t)$ is a Markov process. The evolution is given by the Fokker-Planck equation*

$$\frac{\partial \rho(x,t)}{\partial t} = -\sum_{i=1}^{n} \frac{\partial \left(f_i(x,u_e)\rho(x,t)\right)}{\partial x_i} + \frac{1}{2}\sum_{i=1}^{n}\sum_{j=1}^{n} \frac{\partial^2 \left(g(x)g^T(x)\rho(x,t)\right)_{ij}}{\partial x_i \partial x_j} = A_{FP} \circ \rho(x,t), \quad (3)$$

where A_{FP} is the differential operator the characterizes the evolution of $\rho(x,t)$ with time, also denoted as the Markov transfer operator. For the series of densities $\{\rho_k(x)\} = \{\rho(x,k\tau)\}$ with some $\tau > 0$, the density transfer operator P is a Markov operator such that

$$\rho_{k+1}(x) = P \circ \rho_k(x), \quad (4)$$

and if the Markov process is constrictive [(Lasota & Mackey, 2013, Definition 5.3.1)], then there is a correspondent stationary density $\rho^*(x)$ such that

$$\rho^*(x) = P \circ \rho^*(x). \quad (5)$$

Remark 1 *It is important to note that the Markov transfer operator P completely defines the evolution of the density of the system. Hence, our goal is to analyze the behavior of the AI-driven agents given by* (2)*, through the estimation of the action of P. Our goal is to also estimate the asymptotic behavior of AI-driven agents as several systems* (2) *exhibit stationary states asymptotically. For example, robotics systems are designed to stabilize certain points in the domain. Another example is a diffusion model which is trained to sample from unknown target distributions. For systems that exhibit stationary states, there exists an invariant density ρ^* [Lasota & Mackey (2013)] for the Markov operator such that* (5) *holds. Here agents following* (2) *reach ρ^* asymptotically. We seek to estimate the terminal density ρ^* as it provides a convenient method to assess the alignment of the AI-driven agents.*

Remark 2 *We have noticed that for some general AI agents, the density evolution process of the state may not be a Markovian process. This happens, for example, when $h(x,u)$, $g(x)$ or $u(x)$ in* (1) *and* (2) *are time-variant and non-stationary. In these cases, a similar form of time-variant Fokker-Planck equation holds, though it does not implies a Markov process [Risken (1996)]. Nonetheless, we claim that the Markovian setting is actually widely used and considered for model simplicity and convenience of analysis. To give an example, the state evolution of Markov decision processes (MDPs) with any fixed (stationary) control policy applied, forms a Markov process [Bertsekas (2012)].*

1.4 From Samples to Densities

Our data consists of the state trajectory of N identical agents governed by the dynamics (2). The trajectory of these agents are collected from $t = 0$ to $t = T$ with a fixed sampling period $\tau = \frac{T}{K}$. The sampled dataset is given by $\{\mathcal{X}_n\}_{n=1}^N$ of the state x, where $\mathcal{X}_n = [\chi_0^n, \chi_1^n, \chi_2^n, \cdots, \chi_K^n] \in \mathbb{R}^{M\times(K+1)}$. Note that the collected data set can also come from a single agent starting from N different initial states.

Estimating probability densities from samples is an active problem in machine learning and statistics. In this work, we employ Kernel Density Estimation to numerically construct the probability density $\rho_k(x)$ using the data $\{\mathcal{X}_n\}$. We can view $\{\mathcal{X}_n\}$ by iterating with respect to time as $\{\mathcal{Y}_k\}_{k=0}^K$, where $\mathcal{Y}_k = [\chi_k^1, \chi_k^2, \cdots, \chi_k^N]$ denotes the state vectors of N particles at time $t = k\tau$. Using kernel density estimation [Hastie et al. (2009)], we then get an empirical probability distribution estimation $\rho_k(x)$. In this paper, we choose to use the Gaussian kernel for the estimation of ρ_k which is given by

$$\rho_k(x) = \frac{1}{N\sqrt{\det(2\pi\sigma_k^2 I_M)}} \sum_{n=1}^{N} e^{-\frac{\|x-\chi_k^n\|^2}{2\sigma_k^2}}. \quad (6)$$

It is important to note that any choice of density estimation algorithm can be used with the data $\{\mathcal{X}_n\}$ to obtain $\{\rho_k(x)\}_{k=0}^K$. KDE provides a convenient choice for measuring the probability $\rho(x)$ at fixed reference points. The choice of reference points and the parameter σ_k can be chosen by the user to better approximate ρ_k. In this paper, we choose to uniformly sample the reference points in the domain X to estimate every $\rho_k(x)$. We fix a constant $\sigma_K = \sigma$ for simplicity. More specific KDE-related tools can be used based on the system in consideration and the domain, as enlisted in [Chen (2017)].

We illustrate in Figure 1 how the state trajectory $x(t)$ is coupled with the probability density $\rho(x,t)$ for the Van der Pol oscillator,

$$\dot{x}_1 = x_2, \quad \dot{x}_2 = \mu(1 - x_1^2)x_2 - x_1.$$

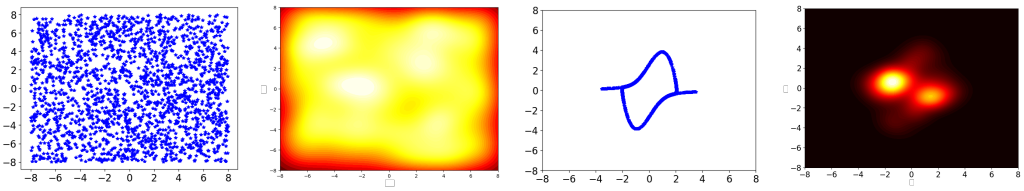

(a) Initial states $x(0)$ (b) Initial density $\rho_0(x)$ (c) States $x(1500\tau)$ (d) Density $\rho_{1500}(x)$

Figure 1: Illustration of the relationship between the states and probability density of the Van der Pol oscillator in a bounded domain. The x-axis in the figures corresponds to x_1 and the y-axis in the figures corresponds to x_2. (a) Various particles with different initial states driven by Van der Pol dynamics. (b) Density of initial state of agents. (c) States of the agent after time $t = 1500\tau$. (d) Density of the states at time $t = 1500\tau$. Brighter colors in (b) and (d) represent higher probability. The states are sampled with $t = 0.01$.

Remark 3 *We acknowledge that the choice of kernels significantly affects both the accuracy and the computational complexity of the algorithm. However, since our main focus lies in predicting the trajectories of densities, we opted for a practical kernel choice tailored to the application at hand. More sophisticated methods to approximate densities from data choosing might yield better results and our algorithm can easily be used with these techniques.*

2 Prediction Informed by Spectral-decomposition Algorithm (PISA) for Learning Markov transfer Operators

We present our algorithm to estimate the Markov transfer operator in this section. Further, we predict the asymptotic behavior of the system by estimating the terminal density of the dynamical system. We approximate the action of the Markov transfer operator using the following model,

$$P \circ \rho_k(x) = \frac{1}{l}\sum_{i=1}^{l} \rho_{k-l+i}(x) - \sum_{i=1}^{l}\left(\frac{1}{l} - \mathtt{A}_\theta^i(\rho_k)\right)\mathtt{G}_\gamma^i(x). \tag{7}$$

Here, we are decomposing the action of the Markov transfer operator on the density $\rho_k(x)$ into $2l$ components as given by l functionals $\mathtt{A}_\theta^i(\rho_k)$ and l functions $\mathtt{G}_\gamma^i(x)$. The functionals $\mathtt{A}_\theta^i(\rho_k)$ and functions $\mathtt{G}_\gamma^i(x)$ are parameterized by θ and γ respectively. Moreover, we impose the following constraints:

$$\begin{aligned} P \circ \mathtt{G}_\gamma^i(x) &= \mathtt{G}_\gamma^{i+1}(x), \quad \forall i = 1, \cdots, l-1; \\ P \circ \mathtt{G}_\gamma^l(x) &= \mathtt{G}_\gamma^1(x); \\ \langle \mathtt{G}_\gamma^i(x), \mathtt{G}_\gamma^j(x) \rangle &= 0, \forall i \neq j. \end{aligned} \tag{8}$$

This method of decomposing the Markov transfer operator is guided by the spectral decomposition theorem which we elaborate on in Section 4.

Given the decomposition of the Markov transfer operator, we propose the following loss function, guided by the spectral decomposition theorem, to learn the parameter θ and γ.

$$L(\theta,\gamma) = \sum_{k=l-1}^{K-1} D\left(\frac{1}{l}\sum_{i=1}^{l}\rho_{k-l+i}(x) - \sum_{i=1}^{l}\left(\frac{1}{l} - \mathtt{A}_\theta^i(\rho_k)\right)\mathtt{G}_\gamma^i(x)\middle\|\rho_{k+1}(x)\right) + \lambda\sum_{i\neq j}^{l}\langle \mathtt{G}_\gamma^i(x), \mathtt{G}_\gamma^j(x)\rangle + \mu\sum_{r=1}^{l} D\left(\sum_{i=1}^{l}\mathtt{A}_\theta^i(\mathtt{G}_\gamma^r)\mathtt{G}_\gamma^i(x)\middle\|\mathtt{G}_\gamma^{r+1}(x)\right) \tag{9}$$

We then construct PISA as the following alternating optimization algorithm to compute θ and γ, in which we choose $\mathtt{A}_\theta^i(\rho)$ and $\mathtt{G}_\gamma^i(x)$ to be outputs of two distinct neural networks parameterized by θ and γ, respectively. An important aspect of PISA is that it can also predict the terminal density of the Markov transfer operator. The estimate of terminal density of P can be expressed as

$$\rho^*(x) = \frac{1}{l}\sum_{i=1}^{l}\mathtt{G}_\gamma^i(x). \tag{10}$$

Algorithm 1: Prediction Informed by Spectral-decomposition Algorithm (PISA)

Data: $l > 0$, $\lambda > 0$, $\mu > 0$; $\rho_k(x)$, for $k = 0, 1, \cdots, K$; initial values of γ and θ; two small positive thresholds ϵ_1 and ϵ_2;

Result: γ and θ;

$N_{\text{epochs}} \leftarrow 1000$

while $N_{epochs} \neq 0$ **do**

  Solve the following optimization problem to get γ^*

$$\min_{\gamma} \;\; L(\theta,\gamma) \quad \text{s.t. } \mathtt{G}_\gamma^i(x) \geq 0 \text{ and } \int \mathtt{G}_\gamma^i(x)dx = 1, \text{ for } i = 1, \cdots, l; \tag{11}$$

  if $\|\gamma^* - \gamma\| \geq \epsilon_1$ **then**

    $\gamma \leftarrow \gamma^*$

  end

  Solve the following optimization problem to get θ^*

$$\min_{\theta} \;\; L(\theta,\gamma) \quad \text{s.t. } \mathtt{A}_\theta^i(\rho_k) \geq 0, \text{ for } i = 1, \cdots, l \text{ and } \sum_{i=1}^{l}\mathtt{A}_\theta^i(\rho_k) = 1; \tag{12}$$

  if $\|\theta^* - \theta\| \geq \epsilon_2$ **then**

    $\theta \leftarrow \theta^*$

  end

  $N_{\text{epochs}} = N_{\text{epochs}} - 1$

end

Note that optimization problems (11) and (12) are constrained by the structure of $\mathtt{G}_\gamma^i$ and $\mathtt{A}_\theta^i$. These constraints are easily satisfied by non-negative output layers of typical neural network architectures. For instance, normalized sigmoid layer for $\mathtt{G}_\gamma^i$ satisfies the constraints in (11) and (12).

3 Numerical Experiments

We present the effectiveness of PISA on different numerical testbeds. We performed the numerical experiments on a machine with Intel i9-9900K CPU with 128GB RAM and the Nvidia Quadro RTX 4000 GPU. In our numerical experiments, we compare the performance of PISA with that of

Meng et al. (2022) and DDPD proposed in Zhao & Jiang (2023). Particularly, Meng et al. (2022) approximates the Perron-Frobenius operator as

$$\rho_{k+1} = e^{t \cdot \mathrm{NN}_\delta(x,t)} \rho_k.$$

Here, note that NN_δ approximates the differential operator A_{FP} given in (3). Then $e^{t \cdot \mathrm{NN}_\delta}$ is an approximately linear solution to (4). Moreover, in Zhao & Jiang (2023), the authors provided the dynamic probability density decomposition (DPDD) method, which is based on Extended Dynamic Mode Decomposition and makes a linear finite-dimensional approximation of the Markov transfer operator to forecast the density evolution.

3.1 Lunar Lander (Continuous)

We apply PISA to predict the behavior of a reinforcement learning algorithm. Lunar lander (Continuous) is a rocket trajectory optimization problem on the Gymnasium platform Towers et al. (2024), with an eight-dimensional state and three-dimensional control input. We first train a feedback control policy using the Actor-Critic algorithm to make the rocket land on the landing pad which is always given by the coordinates (0,0) in the simulation environment. The feedback policy results in stochastic nonlinear dynamics as described in (2). We collect 3000 trajectories of length 500 time steps. We evaluate the density of the states via kernel density estimation (KDE) method to get a trajectory of densities as $\{\rho_t(x)\}_{t=0}^{500}$. We use the first 100 steps of the density trajectory to learn the Markov transfer operator using PISA. We also estimate the Markov transfer operator using DPDD (Zhao & Jiang (2023)), and direct NN (Meng et al. (2022)), respectively to compare the different models. We evaluate the performance of the learned models to predict the density for the following 400 steps to get $\{\hat{\rho}_t(x)\}_{t=101}^{500}$ for each of the three algorithms. We use the KL divergence between the predicted density $\hat{\rho}_k$ and the true density ρ_k to characterize the performance of each algorithm. In Figure 2(a), we compare the performance of the three algorithms. We see that Meng et al. (2022) performs better initially due to its linearity assumption on the transfer operator but PISA performs better in the long term. However, DPDD performs significantly worse as it projects the operator on a finite basis. In Figure 2(b), we depict the predicted stationary density ρ^* of the lunar lander. We see that ρ^* is centered around (0,0) with a high probability which verifies that the controller makes the rocket land within the landing pad most times.

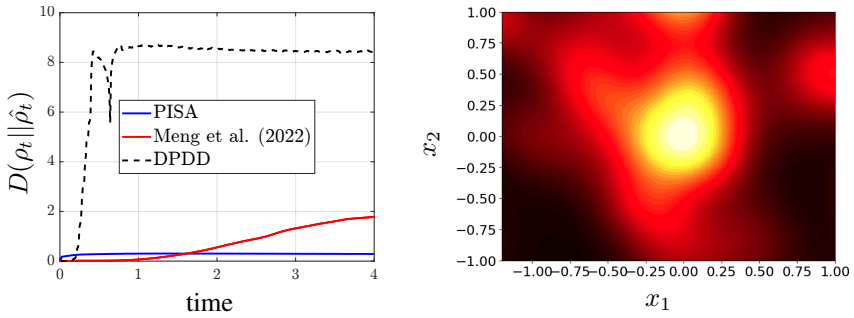

(a) (b)

Figure 2: Experiments on the lunar lander in the Gymnasium environment. (a) Comparison of performance between PISA, Meng et al. (2022) and DPDD. PISA performs better than the other algorithms in the long term although Meng et al. (2022) performs better initially due to its linearity assumption. (b) Prediction of the stationary density ρ^* of the lunar lander centered at (0,0). This confirms that the controller ensures that the rocket lands within the landing pad.

3.2 Predicting Behavior of Score-Based Generative Model

We consider the problem of analysis of the behavior of diffusion models. Diffusion models generate data using a bidirectional scheme. Given data samples from an unknown density, in the forward process, noise is sequentially added until the data samples resemble white noise samples from a standard Gaussian. Then, to generate new samples, the reverse process of diffusion models iteratively removes noise from white noise samples to generate realistic samples from the target density. The

reverse process is particularly complex as the amount of noise to be removed at every step is estimated using neural networks. Our task is to analyze the behavior of diffusion models in the reverse process from the lens of evolving probability densities. We particularly consider the case of diffusion models based on estimating the score Song et al. (2020). We seek to study the behavior of these score-based generative models by their action on samples in the reverse process.

In Song et al. (2020), the forward and reverse processes use the following Stochastic Differential Equation (SDE),

$$\dot{x} = Ax + Bu, \tag{13}$$

where $x, u \in \mathbb{R}^{10}$. In the forward process where noise is sequentially added, $x(0)$are samples from an unknown target distribution, and $u(t)$ is sampled from a Gaussian $u(t) \sim \mathcal{N}(\mathbf{0}, I)$. In the reverse process, $x(T) \sim \mathcal{N}(\mathbf{0}, I)$ is the initial point, and $u(t)$ is the output of a neural network $\mathtt{S}_\psi(x, t)$ that estimates the amount of noise needed to be removed at each step t to obtain a realistic sample. In this experiment, we predict the behavior of the score-based diffusion model in the reverse process. For the reverse process, the task is to sample from Gaussians centered at $-6\mathbf{1}$ and $6\mathbf{1}$ and $k\boldsymbol{I}$ where $k \sim \mathcal{N}(-3, I)$. The noise distribution is the standard Gaussian. In Figure 3(a) we show the first two dimensions of the samples used in the reverse process of the diffusion model. The blue points denote the initial points sampled from a standard Gaussian. The red points denote the final samples from the target distribution. To train the diffusion model, we use $N = 12000$ samples from the target distribution. The data samples are diffused in the forward process for a time period of 8 seconds. In the reverse process, to sample from the desired distributions, we learn the score as proposed in Song et al. (2020). Once the score is sufficiently learned using a neural network, we record N trajectories in the reverse process for a time period of five seconds, which constitute the training dataset. Then we predict the behavior for the next three seconds which is the testing dataset.

We use the KL divergence between the predicted $\hat{\rho}_t$ and the true ρ_t from the testing dataset as a metric to numerically analyze the performance of PISA. It is evident from Figure 3(b) that PISA accurately predicts the behavior of the diffusion model with varying choices of the number of basis functions. We use the logarithm of the KL divergence to emphasize that PISA performs at least one order of magnitude better than the other methods Meng et al. (2022) and DDPD Zhao & Jiang (2023). We see that Meng et al. (2022) performs better initially due to its linear solution to the PDE but its performance deteriorates rapidly. PISA retains relatively much better performance over a longer time horizon. In Figure 3(c), we take a closer look at the performance of PISA for different choices of basis functions l. We see that a choice of $l \geq 10$ is required to achieve good performance. We use feedforward neural networks with 3 hidden layers for $\mathtt{A}^i_\theta$, $\mathtt{G}^i_\gamma$ and $\mathtt{NN}^i_\delta$.

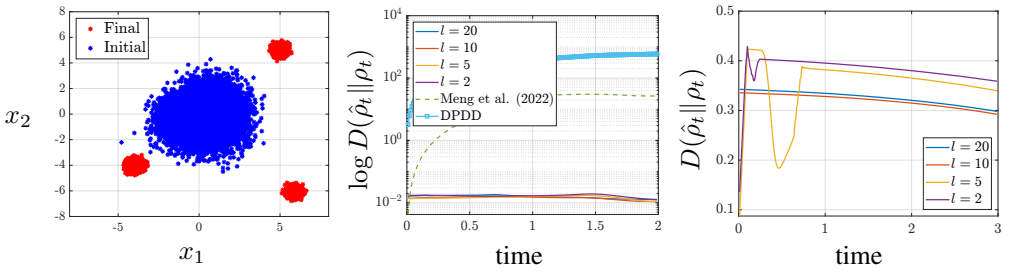

(a) (b) (c)

Figure 3: Experiments on the ten dimensional score-based generative model Song et al. (2020). (a) Data samples of diffusion model. Blue points of the standard Gaussian are the initial points in the reverse process. Red points denote samples from the unknown final distribution. (b) Comparison of performance of PISA with different choices of basis functions l, Meng et al. (2022) and DPDD on testing dataset. PISA performs an order of magnitude better for any choice of basis function. (c) Comparison of PISA with different choices of basis functions l. A choice of $l \geq 10$ is required to achieve the best performance.

3.3 UCY PEDESTRIAN DATASET

Here, we show the effectiveness of PISA on physical data where the transfer operator is not constrictive and the dynamics are not Markov. We apply PISA on the UCY pedestrian dataset Lerner et al. (2007) to predict the movement of pedestrians by estimating the evolution of the density of pedestrians. The dataset consists of videos of pedestrians walking in several regions as depicted in Figure 4(a). We use the Zara01 subsection of the dataset in our experiments. We obtained pre-processed data from the code repository of Salzmann et al. (2020), where the video was processed to obtain the x and y coordinates of the position of the pedestrians. As pedestrians are walking everywhere in state space, the constrictive property no longer holds. Further, pedestrians enter and exit the scene which results in highly stochastic behavior in the density. Given these complications, we show that PISA still performs better than other methods that learn transfer operators. We assume that every pedestrian is identical and their movement is governed by the dynamics given in (2). Both DDPD and Meng et al. (2022) require Markovian dynamics of the density, however we show that PISA can perform well even when this assumption fails.

Given the positions of pedestrians as depicted in Figure 4(a), we approximate the probability density of the pedestrians as depicted in Figure 4(b). In Figure 4(c), we once again compare PISA with the exponential model Meng et al. (2022) on the test data for the first 400 time samples. We choose $l = 5$ and feedforward neural networks with 3 hidden layers for $\mathtt{A}^i_\theta$, $\mathtt{G}^i_\gamma$ and $\mathtt{NN}^i_\delta$. Here, we see that the initial time period in which the exponential model works better than PISA is significantly shorter due to the model inaccuracy. However, PISA continues to perform well over a longer time horizon. It is also important to note that both models have significantly higher estimation errors in the testing performance for this experiment compared to performance in experiments on the Gymnaisum Lunar Lander model and the score-based generative model. This is due to the stochasticity of the data and the assumption we make about the nature of the pedestrians. Better density approximation algorithms that are suited for stochastic data and for incorporating jumps in the probability density can be employed to obtain an improvement in the performance.

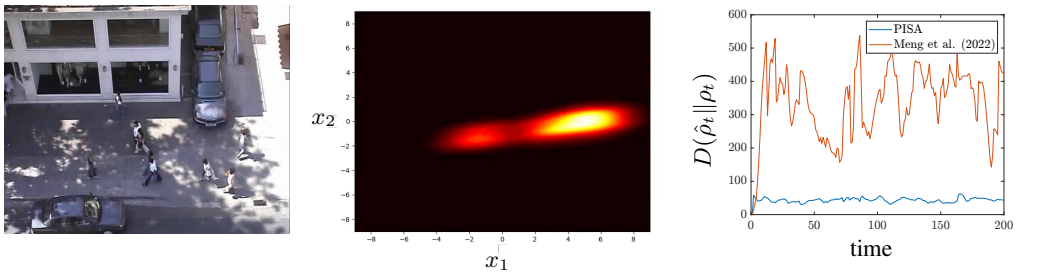

(a) Snapshot from dataset (b) Estimated density ρ_k (c) Comparison with Meng et al. (2022)

Figure 4: Experiments on the UCY pedestrian dataset. (a) A snapshot from the dataset. (b) Corresponding estimated probability density. (c) Comparison between PISA and Meng et al. (2022) in the estimation of future probability densities.

4 THEORETICAL FOUNDATIONS OF SPECTRAL DECOMPOSITION

If the Markov transfer operator P is constrictive, it pushes forward the probability distribution $\rho_k(x)$ to a stationary distribution $\rho^*(x)$ corresponding to the attractors of dynamical systems. This evolution of the probability distribution is in fact a *Markov Process* (see Appendix A). For Markov operators with the constrictive property, we have the following spectral decomposition theorem.

Lemma 2 (Lasota & Mackey (2013)) *Let P be a constrictive Markov operator. Then there exists an integer l, two sequences of non-negative functions $g_i(x) \in \mathcal{L}_1$ and $h_i(x) \in \mathcal{L}_\infty$, $i = 1, 2, \cdots, l$, and an operator $Q : \mathcal{L}_1 \mapsto \mathcal{L}_1$ such that for all $\rho(x) \in \mathcal{L}_1$, $P \circ \rho(x)$ can be written in the form*

$$P \circ \rho(x) = \sum_{i=1}^{l} a_i(\rho) g_i(x) + Q \circ \rho(x), \tag{14}$$

where

$$a_i(\rho) = \int \rho(x) h_i(x) dx.$$

The functions $g_i(x)$ and the operator Q have the following properties:

1) Each $g_i(x)$ is normalized to one and

$$g_i(x) g_j(x) = 0, \quad \textit{for all } i \neq j, \tag{15}$$

i.e., the density functions $g_i(x)$ have disjoint supports;

2) For each integer i there exists a unique integer $\alpha(i)$ such that

$$P \circ g_i(x) = g_{\alpha(i)}(x). \tag{16}$$

where $\alpha(i) \neq \alpha(j)$ for $i \neq j$. Thus, P just permutes the functions $g_i(x)$;

3) Moreover,

$$\| P^n Q \circ \rho(x) \| \to 0 \tag{17}$$

as $n \to \infty$ for every $\rho(x) \in \mathcal{L}_1$.

Lemma 2 states that the action of the PF operator can be decomposed into l components through the functionals $a_i(\rho)$ and the functions $g_i(x)$. Here l is a finite integer that serves as a measure of the model complexity of PISA. Further, the operator Q captures the effect of the terminal density on $\rho(x)$. As $t \to \infty$, the action of Q on $\rho(x)$ decays to 0. This drives our motivation to use $Q \circ \rho(x)$ as

$$Q \circ \rho_k(x) = \frac{1}{l} \sum_{i=1}^{l} \rho_{k-l+i}(x) - \frac{1}{l} \sum_{i=1}^{l} g_i(x). \tag{18}$$

Further, as $t \to \infty$, we can see that

$$\rho^*(x) = \frac{1}{l} \sum_{i}^{l} g_i(x). \tag{19}$$

This implies that the density functions g_i serve as a basis for the stationary terminal density ρ^*. It is easy to verify for (19) that $P \circ \rho^*(x) = \rho^*(x)$ through the permutation property. Given the Lemma 2, (18), and (19), we provide a sufficient condition on the output of our algorithm PISA.

Theorem 1 *For systems* (2) *that have a stationary terminal density, there exists a finite l, an operator Q, l non-negative functionals $\mathbb{A}_\theta^i(\rho)$ and l densities $\mathbb{G}_\gamma(x)$ such that the loss $L(\theta, \gamma) = 0$.*

Proof 1 *We provide a brief overview of the proof. Lemma 2 guarantees the existence of l functions $a_i(\rho)$ and $g_i(x)$ that exactly decompose the action of the PF operator. These are approximated using neural networks $\mathbb{A}_\theta^i(\rho)$ and $\mathbb{G}_\gamma^i(x)$, respectively. The cost function L is designed to satisfy the properties of a_i and g_i. The first term in the cost function L addresses the propagation of the PF operator. The second term addresses the orthogonality property of every g_i and the last term captures the permutative property g_i.* ■

5 Conclusion

In this study, we explore the task of predicting the behavior of agents controlled by AI models, using a probabilistic framework to analyze the evolution of probability densities. Our proposed algorithm, PISA, effectively estimates the Markov transfer operator that characterizes the evolution of these densities, thus enabling predictions of both the short and long-term behavior of AI-driven agents. This ability to forecast asymptotic behaviors is critical for assessing whether such agents align with the controller's requirements. Currently, our approach utilizes kernel density estimation to approximate the probability densities from individual trajectories; however, this method introduces potential inaccuracies. Optimizing the choice of kernel functions and adopting more sophisticated density estimation techniques could significantly enhance our model's performance. Additionally, a comprehensive evaluation of the model's computational efficiency remains to be conducted, which will be crucial for practical applications and further scalability.

REFERENCES

Stefano V Albrecht and Peter Stone. Autonomous agents modelling other agents: A comprehensive survey and open problems. *Artificial Intelligence*, 258:66–95, 2018.

Robert B Ash. *Information theory*. Courier Corporation, 2012.

Tim Baarslag, Mark JC Hendrikx, Koen V Hindriks, and Catholijn M Jonker. Learning about the opponent in automated bilateral negotiation: a comprehensive survey of opponent modeling techniques. *Autonomous Agents and Multi-Agent Systems*, 30:849–898, 2016.

Haoyu Bai, Shaojun Cai, Nan Ye, David Hsu, and Wee Sun Lee. Intention-aware online pomdp planning for autonomous driving in a crowd. In *2015 ieee international conference on robotics and automation (icra)*, pp. 454–460. IEEE, 2015.

Randall D Beer. A dynamical systems perspective on agent-environment interaction. *Artificial intelligence*, 72(1-2):173–215, 1995.

Dimitri Bertsekas. *Dynamic programming and optimal control: Volume I*, volume 4. Athena scientific, 2012.

Steven L Brunton, Marko Budišić, Eurika Kaiser, and J Nathan Kutz. Modern koopman theory for dynamical systems. *arXiv preprint arXiv:2102.12086*, 2021.

Y.-C. Chen. A tutorial on kernel density estimation and recent advances, 2017.

T. De Ryck and S. Mishra. Generic bounds on the approximation error for physics-informed (and) operator learning. *Advances in Neural Information Processing Systems*, 35:10945–10958, 2022.

Grégoire Déletang, Jordi Grau-Moya, Miljan Martic, Tim Genewein, Tom McGrath, Vladimir Mikulik, Markus Kunesch, Shane Legg, and Pedro A Ortega. Causal analysis of agent behavior for ai safety. *arXiv preprint arXiv:2103.03938*, 2021.

Das Dipta, Ihsan Ibrahim, and Naoki Fukuta. Observing and understanding agent's characteristics with environmental changes for learning agents. In *2022 12th International Congress on Advanced Applied Informatics (IIAI-AAI)*, pp. 424–429. IEEE, 2022.

Prashant Doshi and Piotr J Gmytrasiewicz. A particle filtering based approach to approximating interactive pomdps. In *AAAI*, pp. 969–974, 2005.

M. Everett, G. Habibi, C. Sun, and J. P. How. Reachability analysis of neural feedback loops. *IEEE Access*, 9:163938–163953, 2021.

Sam Ganzfried and Tuomas Sandholm. Game theory-based opponent modeling in large imperfect-information games. In *The 10th International Conference on Autonomous Agents and Multiagent Systems-Volume 2*, pp. 533–540, 2011.

Crispin Gardiner. *Stochastic methods*, volume 4. Springer Berlin Heidelberg, 2009.

D. Goswami, E. Thackray, and D. A. Paley. Constrained ulam dynamic mode decomposition: Approximation of the perron-frobenius operator for deterministic and stochastic systems. *IEEE control systems letters*, 2(4):809–814, 2018.

Y. Hashimoto, M. Ikeda, and H. Kadri. Deep learning with kernels through rkhm and the perron-frobenius operator. *Advances in Neural Information Processing Systems*, 36, 2024.

T. Hastie, R. Tibshirani, and J. H. Friedman. *The elements of statistical learning: data mining, inference, and prediction*, volume 2. Springer, 2009.

J. Ho, A. Jain, and P. Abbeel. Denoising diffusion probabilistic models. *Advances in neural information processing systems*, 33:6840–6851, 2020.

Bret Hoehn, Finnegan Southey, Robert C Holte, and Valeriy Bulitko. Effective short-term opponent exploitation in simplified poker. In *AAAI*, volume 5, pp. 783–788, 2005.

C. Huang, J. Fan, W. Li, X. Chen, and Q. Zhu. Reachnn: Reachability analysis of neural-network controlled systems. *ACM Transactions on Embedded Computing Systems (TECS)*, 18(5s):1–22, 2019.

Auke Jan Ijspeert, Jun Nakanishi, and Stefan Schaal. Movement imitation with nonlinear dynamical systems in humanoid robots. In *Proceedings 2002 IEEE International Conference on Robotics and Automation (Cat. No. 02CH37292)*, volume 2, pp. 1398–1403. IEEE, 2002.

Amirhossein Karimi and Tryphon T Georgiou. Data-driven approximation of the perron-frobenius operator using the wasserstein metric. *IFAC-PapersOnLine*, 55(30):341–346, 2022.

Diederik P Kingma. Auto-encoding variational bayes. *arXiv preprint arXiv:1312.6114*, 2013.

A. Lasota and M. C. Mackey. *Chaos, fractals, and noise: stochastic aspects of dynamics*, volume 97. Springer Science & Business Media, 2013.

Seong Jae Lee and Zoran Popović. Learning behavior styles with inverse reinforcement learning. *ACM transactions on graphics (TOG)*, 29(4):1–7, 2010.

Stéphanie Lefèvre, Dizan Vasquez, and Christian Laugier. A survey on motion prediction and risk assessment for intelligent vehicles. *ROBOMECH journal*, 1:1–14, 2014.

A. Lerner, Y. Chrysanthou, and D. Lischinski. Crowds by example. In *Computer graphics forum*, volume 26, pp. 655–664. Wiley Online Library, 2007.

Sergey Levine, Chelsea Finn, Trevor Darrell, and Pieter Abbeel. End-to-end training of deep visuomotor policies. *Journal of Machine Learning Research*, 17(39):1–40, 2016.

Z. Li, H. Zheng, N. Kovachki, D. Jin, H. Chen, B. Liu, K. Azizzadenesheli, and A. Anandkumar. Physics-informed neural operator for learning partial differential equations. *ACM/JMS Journal of Data Science*, 2021.

Y. Meng, D. Sun, Z. Qiu, M. T. B. Waez, and C. Fan. Learning density distribution of reachable states for autonomous systems. In *Proceedings of the 5th Conference on Robot Learning*, volume 164 of *Proceedings of Machine Learning Research*, pp. 124–136. PMLR, 08–11 Nov 2022.

Kumpati S Narendra and Kannan Parthasarathy. Neural networks and dynamical systems. *International Journal of Approximate Reasoning*, 6(2):109–131, 1992.

R. A. Norton, C. Fox, and M. E. Morrison. Numerical approximation of the frobenius–perron operator using the finite volume method. *SIAM Journal on Numerical Analysis*, 56(1):570–589, 2018.

Shokoofeh Pourmehr and Chitra Dadkhah. An overview on opponent modeling in robocup soccer simulation 2d. *RoboCup 2011: Robot Soccer World Cup XV 15*, pp. 402–414, 2012.

Amir Rasouli, Iuliia Kotseruba, and John K Tsotsos. Understanding pedestrian behavior in complex traffic scenes. *IEEE Transactions on Intelligent Vehicles*, 3(1):61–70, 2017.

H Risken. The fokker-planck equation, 1996.

Francesca Rossi and Nicholas Mattei. Building ethically bounded ai. In *Proceedings of the AAAI Conference on Artificial Intelligence*, volume 33, pp. 9785–9789, 2019.

Nicholas A Roy, Junkyung Kim, and Neil Rabinowitz. Explainability via causal self-talk. *Advances in Neural Information Processing Systems*, 35:7655–7670, 2022.

T. Salzmann, B. Ivanovic, P. Chakravarty, and M. Pavone. Trajectron++: Dynamically-feasible trajectory forecasting with heterogeneous data. In *Computer Vision–ECCV 2020: 16th European Conference, Glasgow, UK, August 23–28, 2020, Proceedings, Part XVIII 16*, pp. 683–700. Springer, 2020.

Peter J Schmid. Dynamic mode decomposition and its variants. *Annual Review of Fluid Mechanics*, 54(1):225–254, 2022.

Y. Song, J. Sohl-Dickstein, D. P. Kingma, A. Kumar, S. Ermon, and B. Poole. Score-based generative modeling through stochastic differential equations. *arXiv preprint arXiv:2011.13456*, 2020.

S. Surasinghe, J. Fish, and E. M. Bollt. Learning transfer operators by kernel density estimation. *Chaos: An Interdisciplinary Journal of Nonlinear Science*, 34(2), 2024.

Wesley Suttle, Vipul Kumar Sharma, Krishna Chaitanya Kosaraju, Sivaranjani Seetharaman, Ji Liu, Vijay Gupta, and Brian M Sadler. Sampling-based safe reinforcement learning for nonlinear dynamical systems. In *International Conference on Artificial Intelligence and Statistics*, pp. 4420–4428. PMLR, 2024.

M Towers, A. Kwiatkowski, J. Terry, J. U. Balis, G. De Cola, T. Deleu, M. Goulão, A. Kallinteris, M. Krimmel, A. KG, et al. Gymnasium: A standard interface for reinforcement learning environments. *arXiv preprint arXiv:2407.17032*, 2024.

Pete Trautman, Jeremy Ma, Richard M Murray, and Andreas Krause. Robot navigation in dense human crowds: Statistical models and experimental studies of human–robot cooperation. *The International Journal of Robotics Research*, 34(3):335–356, 2015.

Y. Yang, L. Nurbekyan, E. Negrini, R. Martin, and M. Pasha. Optimal transport for parameter identification of chaotic dynamics via invariant measures, 2022.

C. Zhang, W. Ruan, and P. Xu. Reachability analysis of neural network control systems. In *Proceedings of the AAAI Conference on Artificial Intelligence*, volume 37, pp. 15287–15295, 2023.

M. Zhao and L. Jiang. Data-driven probability density forecast for stochastic dynamical systems. *Journal of Computational Physics*, 492:112422, 2023.

A OPERATOR THEORY AND STATISTICAL MECHANICS

The study of density evolution from a macroscopic perspective is rooted in the principles of statistical mechanics, which bridge the microscopic behavior of individual components and the macroscopic properties of complex systems. Foundational works, such as those by Lasota & Mackey (2013) and Risken (1996), have established frameworks for examining how distributions of states evolve over time in systems governed by stochastic dynamics. This perspective is particularly valuable in systems with high-dimensional, nonlinear dynamics, such as AI-driven agents, where direct analysis of individual trajectories is impractical.

The macroscopic approach shifts focus from tracking each particle or agent to analyzing the aggregate behavior of a population. By modeling the evolution of probability densities, this framework enables predictions about the statistical behavior of the system as a whole, revealing regularities that emerge despite underlying stochasticity and chaos. A crucial simplification in this framework is the assumption of independence among trajectories.

Assumption 1 (Ash (2012)) *(Independent Particles Approximation) In our basic problem setting, we assume that there are N trajectories indexed by n and each trajectory $\mathcal{X}_n = [\chi_0^n, \chi_1^n, \chi_2^n, \cdots, \chi_K^n] \in \mathbb{R}^{M\times(K+1)}$ is generated independently and governed by the identical systems dynamics as shown in* (2).

This assumption, inspired by the ideal gas model in thermodynamics, allows the collective behavior of the system to be captured using a single probabilistic model. This i.i.d. (independent and identically distributed) assumption significantly reduces analytical complexity. While it assumes independence, it remains applicable in practical scenarios where trajectories exhibit weak correlations, a common feature in many real-world systems. For instance, trajectories can be treated as independent samples from multiple agents or as repeated simulations of the same agent under varying initial conditions.

By adopting this assumption, we unify the analysis into a single macroscopic model: the stochastic process $\{\rho_k(x)\}_{k=0}^{\infty}$, which represents the evolution of probability densities over time. This abstraction allows us to study the system's collective behavior at a higher level, avoiding the need to track each particle or agent individually.

As shown in Section 1.3 and Lemma 1, for trajectories collection we consider in this paper, the density evolution chain $\{\rho_k(x)\}_{k=0}^{\infty}$ forms a Markov process (Markov chain). Next, we will introduce some basic properties of Markov processes (chains) and Markov operators.

Definition 1 (Ash (2012); Lasota & Mackey (2013)) *In probability theory and statistics, a (discrete) Markov chain or Markov process is a stochastic process $\{\rho_k(x)\}_{k=0}^{\infty}$ describing the evolution of states $x \in \mathbb{R}^M$, in which the state at time instant k depends only on the state attained in the previous event x_{k-1}. In operator theory, a Markov operator propagates densities as, that is $P \circ \rho_k(x) = \rho_{k+1}(x)$. Here, P is a linear operator on a certain function space (positive $\mathcal{L}_1$ function space) that conserves the $\mathcal{L}_1$ norm (the so-called Markov property).*

In other words, for the corresponding Markov transfer operator P that propagates the density $\rho_k(x)$ forward, we have that [Lasota & Mackey (2013)]

- P is a linear operator;
- $P \circ \rho(x)$ is non-negative if $\rho(x)$ is non-negative;
- Integral invariance: For $\rho(x) \geq 0$,

$$\int P \circ \rho(x)dx = \int \rho(x)dx;$$

Many practical systems, especially those involving controlled stochastic dynamics, exhibit a special property known as constrictiveness. A constrictive Markov process is one that asymptotically converges to a group of periodical densities $\{g_i(x)\}_{i=1}^{l}$ [Lasota & Mackey (2013)]. It is obvious that this class of Markov chains have a stationary density $\rho^*(x) = \frac{1}{l}\sum_{i=1}^{l} g_i(x)$ and this stationary density satisfies the fixed-point equation [Lasota & Mackey (2013)]:

$$P \circ \rho^*(x) = \rho^*(x).$$

This stationary density represents the long-term behavior of the system, encapsulating its equilibrium state. For instance, in a controlled robotic system, $\rho^*(x)$ might describe the distribution of stable states achieved under a given control policy. The existence of $\rho^*(x)$ has profound implications:

- It provides a concrete representation of the system's asymptotic behavior.
- It enables assessment of system alignment with desired objectives. For example, a generative AI model trained to sample from a specific distribution can be evaluated by comparing its stationary density $\rho^*(x)$ to the target distribution.

This macroscopic approach to density evolution has broad applications in AI and robotics. By focusing on the evolution of probability densities, we can predict and analyze the behavior of complex systems without explicitly modeling individual components. For example:

- Robotics: Assessing the stability and reliability of control policies.
- Generative AI: Evaluating sampling processes in diffusion-based models.
- Crowd Dynamics: Understanding collective motion in human or animal groups.

Furthermore, this framework offers computational advantages. Directly tracking individual trajectories in high-dimensional systems is often infeasible due to the curse of dimensionality. Instead, modeling the evolution of densities provides a scalable and efficient alternative.

B HYPERPARAMETER OF PISA IN EXPERIMENTS

Hyperparameters of PISA in Different Experiments			
Hyperparameter	Lunar Lander	Score-Based Generative Model	UCY Pedestrian
λ	5×10^{-4}	5×10^{-4}	5×10^{-4}
μ	5×10^{-4}	5×10^{-4}	5×10^{-4}
l	5	5 (2, 10, 20 for comparison)	5
N_{epochs}	1000	1000	1000
Optimization Method	Adam	Adam	Adam
Learning Rate	5×10^{-3}	5×10^{-3}	5×10^{-3}
K	100	500	600
Hidden Layers of $\mathbb{A}_\theta^i(\rho)$ and $\mathtt{G}_\gamma^i(x)$	3	3	3
Kernel used in KDE	Gaussian Kernel	Gaussian Kernel	Gaussian Kernel
Bandwidth	1.0	0.8	0.6
Number of Sample Trajectories (N)	3000	5000	400
Number of Reference Points (N_{ref}) for KDE	3000	3000	3000

Remark 4 *Note that we set low values for λ and μ because we give a higher preference for short-term predictions of the density evolution. The parameters λ and μ particularly consider the properties necessary to estimate the terminal behavior of the Markov transfer operator.*